RSC Advances

PAPER

View Article Online
View Journal | View Issue

Cite this: *RSC Adv.*, 2019, **9**, 18902

Controllable synthesis of three-dimensional nitrogen-doped hierarchical porous carbon and its application in the detection of lead†

Runying Dai, * Xue Ma, Quan Xu and Limin Lu*

In this study, gelatin-based microcapsules were first proposed as a carbon source for the synthesis of nitrogen-doped hierarchical porous carbon (N-HPC) *via* a facile one-pot high-temperature treatment. The morphologies of the microcapsules could be well controlled by adjusting the synthesis parameters; this ensured the repeatability of the calcined products. The as-prepared N-HPC possesses a favorable three-dimensional network structure and hierarchical porous structure. As a promising modified electrode, N-HPC displayed remarkably improved stability and sensitivity for lead ion (Pb^{2+}) detection. Moreover, two factors are responsible for the good analytical performance: (i) the morphologies of the microcapsules are controllable and reproducible; this improves the detection stability; and (ii) the nitrogen atoms in the shells of the microcapsules can efficiently interact with Pb^{2+}; this enhances the detection sensitivity. The influences of various experimental parameters, including the pH value of the supporting electrolyte, deposition potential and deposition time, on the stripping signal of Pb^{2+} were investigated. The method displayed a wide linear range of the Pb^{2+} concentration from 7 nM to 7000 nM with the detection limit of 1.44 nM under the optimized conditions. The modified electrode possessed high selectivity, which might be due to the high binding affinity of the NH_2^- groups to Pb^{2+}. The developed method has been successfully applied to the detection of Pb^{2+} in actual water samples; this demonstrates that the N-HPC-based electrochemical sensors have prospective applications in the environmental monitoring of Pb^{2+}.

Received 25th March 2019
Accepted 29th May 2019

DOI: 10.1039/c9ra02270h

rsc.li/rsc-advances

Introduction

Heavy metal pollution causes significant damage to the environment and human health. Lead (Pb^{2+}) is one of the highly poisonous metals, which can be deposited in plants and animals and ultimately harms human health by transfer *via* the food chain. Small amounts of Pb^{2+} may have severe effects on the human soft tissues, blood, organs, bone and immune system.[1,2] The World Health Organization (WHO) has designated the maximum allowable limit of 10 ppb (48 nM) for Pb^{2+} in drinking water.[3] Consequently, the quantitative determination of Pb^{2+} in the environment is important.

To date, various techniques, such as atomic absorption spectroscopy,[4] inductively coupled plasma mass spectrometry,[5] ion chromatography,[6] surface enhanced Raman spectrometry,[7] and electrochemical methods,[8] have been widely used in the detection and monitoring of Pb^{2+}. Among them, electrochemical methods are considered as a valid technique for the trace determination of heavy metal ions due to their good selectivity, high sensitivity, fast response and convenience.[9,10] The key to electrochemical sensing technique is the enrichment of target ions on the surface of a working electrode and electron transfer between the composite material and the electrode. Therefore, the selection of suitable materials to construct the electrode interface has a significant influence on the sensing performance.

Carbon nanomaterials, especially carbon with a three-dimensional (3D) heterostructure, are considered to be unique and attractive electrode modification materials due to their fast electron transfer and large specific surface area.[9,11–13] Wang *et al.* prepared a novel supporting material for an electrochemical sensing platform using three-dimensional macroporous carbon (3D-KSCs) obtained from kenaf stem (KS).[14] The 3D-KSC-modified electrode had a 3D honeycomb porous structure and exhibited good electrochemical behavior for the reduction or oxidation of H_2O_2, glucose and amino acids.[14] Qiu *et al.* developed a 3D graphene/sodium dodecyl benzene sulfonate hemimicelle (GF/SDBS HM) composite electrode. The GF/SDBS HM-based sensor exhibited excellent peel performance in Pb^{2+} analysis, and the detection limit was 0.0145 nM, which could be ascribed to the unique accumulation and deposition

Key Laboratory of Crop Physiology, Ecology and Genetic Breeding, Ministry of Education, Institute of Functional Materials and Agricultural Applied Chemistry, College of Science, Jiangxi Agricultural University, Nanchang 330045, PR China. E-mail: runyingdai@163.com; lulimin816@hotmail.com

† Electronic supplementary information (ESI) available. See DOI: 10.1039/c9ra02270h

behavior of the 3D graphene foam.[15] Although the above mentioned 3D carbon materials showed significant electrochemical behavior, their morphologies were unpredictable; this might result in poor electrode reproducibility. Thus, a method for the controllable preparation of a 3D carbon nanomaterial is highly required.

To date, the template method has been demonstrated to be an effective approach to obtain 3D heterostructured carbon. For example, recently, Deng *et al.* reported 3D graphene-like carbon frameworks (3DGLCFs) with high specific surface area and high content of nitrogen dopant. For the sensing of ascorbic acid, dopamine and uric acid, the current response at the 3DGLCF electrode was much higher than that at commercial graphene.[16] Liu *et al.* prepared porous graphene-like carbon materials (PGCMs) using petroleum pitch as a carbon source and nano-$CaCO_3$ as a template. At 0.5 A g^{-1}, the obtained materials displayed the high surface area and specific capacitance of 899 m^2 g^{-1} and 218.75 F g^{-1}, respectively.[17] Indeed, these methods show high controllability and reproducibility; however, complex steps are required for template removal; hence, the development of a controllable and reproducible synthetic method in a simple and green fashion remains a significant challenge.

Microcapsules, a kind of core–shell structure materials, can be commonly obtained by *in situ* polymerization, interfacial polymerization, spray drying, solvent evaporation, and complex coacervation. Compared to other methods, complex coacervation is simple and efficient, and the involved raw materials, such as gelatin, gum arabic, chitosan, *etc.*, are also very cheap.[18] Especially, the morphologies of gelatin-based microcapsules can be easily controlled by adjusting the synthesis parameters.[19–21] Moreover, note that the gelatin-based microcapsules are rich in N atoms, which have high electronegativity and exhibit strong metal ion-coordinating ability. Thus, it is expected that microcapsules would be ideal precursors for the preparation of N-doped 3D porous carbons, which can be regarded as an excellent electrochemical sensing platform for the detection of heavy metals.

Herein, for the first time, nitrogen-doped 3D hierarchical porous carbon (N-HPC) was synthesized *via* a simple one-pot high-temperature treatment by adopting gelatin-based microcapsules as the carbon source without any additional template. The obtained N-HPC was used as an efficient sensing material for the detection of Pb^{2+} using the differential pulse anodic stripping voltammetry (DPASV) method. Due to strong coordination between Pb^{2+} and the N atoms in N-HPC and large specific surface area of N-HPC, the N-HPC-modified electrode significantly improved the sensitivity and selectivity of the sensor towards Pb^{2+} detection. Moreover, the modified electrode showed superior reproducibility, stability, and repeatability.

Experimental

Materials

Gelatin (GE, isoelectric point pH, pI = 4.7) was purchased from Qunli Gelatin Chemical Co. (Hangzhou, China). Sodium carboxymethyl-cellulose (NaCMC), acetic acid and glutaraldehyde (25 wt%) were purchased from Aladdin Reagent Co. (Shanghai, China). Nitric acid, tetrachloroethylene, HAc and NaAc were bought from Tianjin Damao Chemical Reagent Factory (Tianjin, China). Dioctyl sulfosuccinate sodium (DSS) was produced by Shanghai Chuanxin Chemical Co. Ltd (Shanghai, China). At pH values of 3.0–8.0, the effect of the supporting electrolyte was studied by using HAc–NaAc buffer solutions. The preserved Pb^{2+} solutions were fabricated by diluting $PbCl_2$ with the 0.1 M HNO_3 solution. Distilled water was used in all experiments. All chemicals were directly employed and required no purification.

Apparatus

The optical microscopy (OM, BX-51, Olympus Co., Japan) and scanning electron microscopy (SEM, S-3400N, Hitachi Co., Japan) were used for characterizing the morphologies of the GE/NaCMC/DSS microcapsules (GMs). Energy dispersive X-ray spectroscopy (EDX, EMAX X-act, Horiba Co., Japan) was used to analyze the elements of the N-HPC. An adopting laser particle size analyzer (LS 13320, Beckman Coulter Co., USA) was used to measure the particle size distribution of the GMs. The thermal behavior of the GMs was measured on a thermogravimetric analyzer (TGA, TGA 4000, PerkinElmer Co. USA). The GMs were carbonized in a vacuum tube furnace (SKGL-1200C, Shanghai Jvjing Precision Instrument Manufacturing Co., China). The GMs were freeze-dried in vacuum (FD-1A-50, Beijing Boyikang Experimental Instrument Co., China). An electrochemical workstation (ECW, CHI 660D, Shanghai Chen Hua instruments Co., China) was used to record the electrochemical tests. The three-electrode system was comprised of an auxiliary electrode, reference electrode (SCE) and working electrode. The working electrode was the modified electrode.

Preparation of microcapsules by complex coacervation

GE/NaCMC/DSS microcapsules, which belong to the gelatin-based microcapsules (GMs), were made according to a previous publication with some modifications.[22] Briefly, the GMs were prepared with 14 g GE (10%, w/v), 40 g NaCMC (0.5%, w/v) and 0.0267 g (0.6 mM) dioctyl sulfosuccinate sodium (DSS) and the shell materials were prepared by dissolving in distilled water, which was stirred (250 rpm) in a water bath (40 °C) for 1 h. 12 g of a tetrachloroethylene suspension served as the core material and was quickly added into the shell materials to form the mixture solution, which was stirred at 250 rpm. The complex coacervates were formed when the pH of the mixture solution was lower than the pI of the gelatin solution. After the temperature was slowly cooled to below 5 °C, 2.0 g glutaraldehyde (25%) as a crosslinker was added to the complex coacervates. After washing with distilled water, the obtained microcapsules were freeze dried.

N-HPC modified GCE (N-HPC/GCE)

The GCE (Φ = 3 mm) was buffed with a ruthenium containing lithium oxide, cleaning with distilled water, then drying at room temperature prior to modification.

The nitrogen-doped 3D hierarchical porous carbon (N-HPC) was obtained *via* carbonizing the above prepared GMs at high

temperature. A 1.0 mg mL^{-1} N-HPC suspension solution was prepared by dispersing 2.0 mg N-HPC in a 2.0 mL aqueous solution. The N-HPC suspension solution was sonicated for 30 minutes, and then 5 μL of the N-HPC suspension was spun on the GCE surface. Finally, the N-HPC-modified GCE (N-HPC/GCE) was air dried before use.

Electrochemical determination for Pb^{2+}

All of the electrochemical tests were executed in 0.1 M HAc-NAc buffer solution containing a certain amount of Pb^{2+} at pH 5.0. Pb^{2+} was deposited on the N-HPC/GCE surface for 300 s with a deposition potential of −0.8 V in an agitated solution. Differential pulse anodic stripping voltammetry (DPASV) was adopted to detect Pb^{2+}, tested in the potential range of −0.8 V–0.6 V with the following test parameters: 50 mV amplitude, 50 ms pulse width, 4 mV potential step, 0.2 s pulse period, 16.7 ms sample width, and 2 s quiet time. Prior to the next measurement, a "cleaning" step was performed as follows: N-HPC/GCE was immersed in 0.1 M HAc–NaAc buffer solution with a pH of 5.0. Then, a chronoamperometric technique with a potential of +0.3 V was performed on N-HPC/GCE for 150 s. All the tests were performed in air at room temperature.

Results and discussion

Characterization of GMs and N-HPC

The FTIR spectrum of the obtained N-HPC is shown in Fig. S1.† The big peak located at 3421 cm^{-1} corresponds to the stretching vibration of –NH. The peaks at 2922 cm^{-1} and 2853 cm^{-1} are attributed to the asymmetric and symmetric stretching vibrations of $-CH_2$, respectively. The peaks at 1460 cm^{-1} and 1399 cm^{-1} are assigned to the asymmetric and symmetric stretching vibrations of $-CH_3$, respectively. The peak at 1056 cm^{-1} is attributed to the C–O–C stretching vibration.

Fig. 1 shows the surface morphology and the particle size distribution of the microcapsules obtained using GE/NaCMC/DSS at pH 4.5. The gelatin microcapsules (GMs) had a good appearance and were optically transparent (Fig. 1a). A uniform particle size of the GMs and the mean diameter of 6.75 μm were observed, as shown in Fig. 1b. Fig. 1c demonstrates a cross-section image of the GMs. The shell materials of the microcapsules were composed of many uniform micropores with the pore size of about 6.5 μm. The microcapsules exhibited shrinkage due to the removal of water. Fig. 1d displays a cross-section image of N-HPC. Compared with the GMs, the shell materials of the microcapsules shrunk after calcination, and the pore size of the microcapsules decreased to about 1.2 μm. The TEM image in Fig. S2† exhibits that N-HPC is composed of carbon thin films with macropores or mesopores, which would be favorable for the adsorption of target ions.

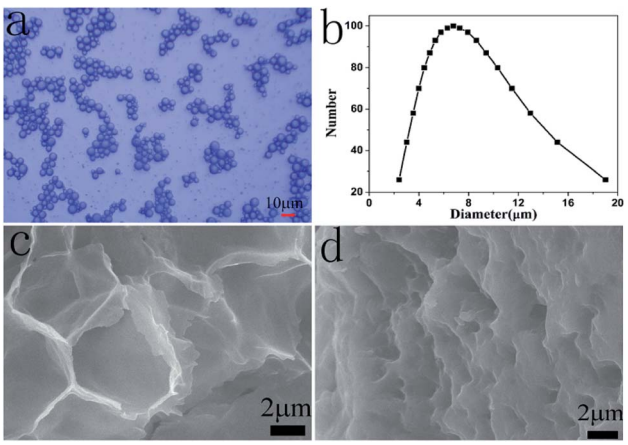

Fig. 1 Surface morphology and particle size distribution of the microcapsules: (a) OM of GMs; (b) particle size distribution of GMs; (c) SEM of GMs; and (d) SEM of N-HPC.

Fig. 2 shows the thermal stability of the GMs as a function of temperature. The gradual weight loss of 1.74% represents the volatilization of water in the microcapsules before 100 °C. The sharp weight loss of 77.32% between 100 °C and 480 °C may represent the decomposition of the core materials including tetrachloroethylene. At 480–640 °C, the weight loss of 18.10% may be attributed to the decomposition of the shell materials of the microcapsules, which suggests that the shell materials can be carbonized at temperatures higher than 640 °C. Therefore, N-HPC was formed at the temperature of 650 °C in 6 h with the GMs.

The XRD pattern of N-HPC is shown in Fig. S3.† A broad peak around 25° in the XRD pattern is indexed as the (002) reflection, which can be attributed to the non-crystallite components present in N-HPC. Moreover, the XRD pattern has sharp peaks at around 32°, 46° and 50°, which can be ascribed to the crystallite components in N-HPC. The crystalline structure confers good electrochemical properties to N-HPC.

Electrochemical characterization of the electrochemical sensor

Electrochemical impedance spectroscopy (EIS) was applied to characterize the modified electrode interface. The electron transfer resistance R_{et} can be derived from the diameter of the semicircle in the high frequency region of the EIS spectrum;[23,24] Fig. S4† shows that the R_{et} of the N-HPC/GCE (b) is smaller than that of bare GCE (a); this is due to the fact that N-HPC with good conductivity increases the electron transfer of $[Fe_3(CN)_6]$ on the surface of the electrode.

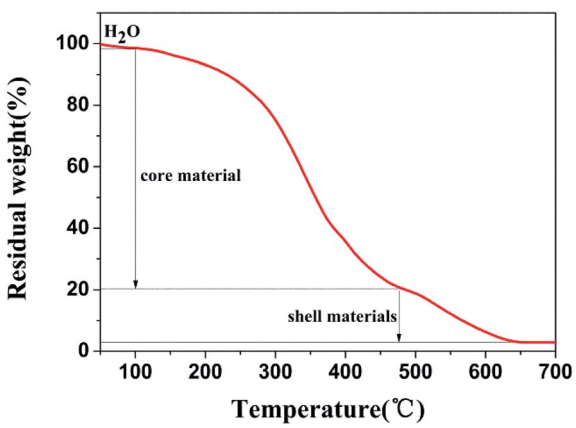

Fig. 2 Thermogravimetric analysis of GMs.

The effective surface area curves of the bare GCE and N-HPC/GCE as a function of time are shown in Fig. 3. The effective surface area of the modified electrode was determined using 1 μM $K_3[Fe(CN)_6]$ as a model complex by the chrono-coulomb method. The Anson equation[25] applied herein is as follows:

$$Q(t) = \frac{2nFAcD^{\frac{1}{2}}t^{\frac{1}{2}}}{\pi^{\frac{1}{2}}} + Q_{dl} + Q_{ads}$$

where n is the number of electrons transferred during the electrode reaction; F is the Faraday constant (96.485 C mol^{-1}); c is the substrate concentration; D refers to the diffusion coefficient of $K_3[Fe(CN)_6]$ in 1.0 M KCl (7.6×10^{-6} cm^2 s^{-1}); and Q_{dl} and Q_{ads} are the double-layer charge and surface charge, respectively. The effective surface areas of the bare GCE and N-HPC/GCE were estimated to be 0.0190 cm^2 and 0.0273 cm^2, respectively. The effective surface area of the N-HPC/GCE was bigger than that of the bare GCE. These results confirm that the N-HPC materials have large surface area, which is favorable for the adsorption of target ions.

Fig. 4 shows the electrochemical behaviors of the bare electrode and N-HPC/GCE in a 0.1 M HAc–NaAc buffer solution at pH 5.0 containing 5.0 μM Pb^{2+}. As shown, the stripping peak was observed for Pb^{2+} at the bare GCE (curve a). Importantly, a sharper stripping peak with obviously improved current for Pb^{2+} is exhibited by the N-HPC/GCE (curve b), which may be attributed to the superior effective specific surface area and satisfactory electrical conductivity of N-HPC. In addition, high density N-containing groups on N-HPC can effectively bind to Pb^{2+}, as confirmed by EDX. As shown in Fig. 5, the C and N peaks were obviously detected in the EDX spectrum of N-HPC before and after its interaction with Pb^{2+}. The magnified images (curve b) show additional distinct Pb peaks at 1.74 keV, 2.36 keV and 2.63 keV for N-HPC after the adsorption of Pb^{2+}, which indicate that the N-HPC-modified GCE has successfully adsorbed Pb^{2+}.

Optimization of the experimental parameters

The influence of the pH value on the stripping peak current was investigated in the range of 3.0–8.0 by DPASV in the HAc–NaAc buffer solution containing 1.0 mM Pb^{2+}. Fig. 6a demonstrates that the peak current of Pb^{2+} increases as the pH increases from 3.0 to 5.0; this may be due to strong complexation between the NH_2^- groups from N-HPC and Pb^{2+}.[26] When the pH was further increased to 8.0, the peak current conversely decreased; this could be attributed to the precipitation of $Pb(OH)_2$ from the solution.[8] Therefore, the HAc–NaAc buffer solution pH of 5.0 was selected as the optimal condition in this study.

The effect of deposition potential on the stripping peak currents of Pb^{2+} at the deposition time of 300 s was investigated between −0.4 and −1.4 V *vs.* the SCE. Fig. 6b reveals that the peak current of Pb^{2+} improves remarkably as the deposition potential shifts from −0.4 V to −0.8 V. As the deposition potential shifts to more negative values, the peak current decreases due to hydrogen evolution.[27] Hence, −0.8 V was chosen as the best deposition potential.

The effect of accumulation time on the stripping peak current of Pb^{2+} was studied at the deposition potential of −0.8 V. As shown in Fig. 6c, the peak current response increased with an increase in the deposition time from 50 to 350 s.

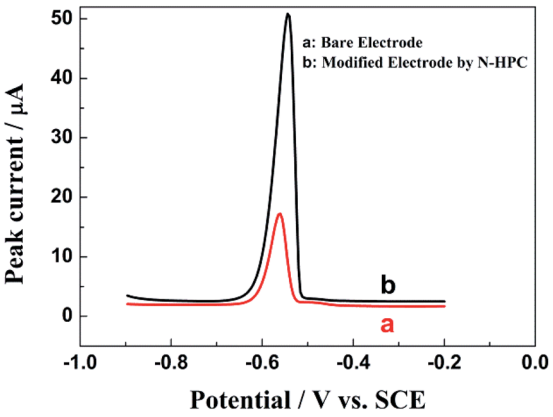

Fig. 4 The DPASV curves of the bare GCE (a) and N-HPC/GCE (b) in a 0.1 M HAc–NaAc buffer solution at pH 5.0 containing 5.0 μM Pb^{2+}. Deposition potential: −0.8 V; amplitude: 50 mV; potential step: 4 mV; deposition time: 350 s; pulse period: 0.2 s; pulse width: 50 m s; sample width: 0.0167 s; and quiet time: 2 s.

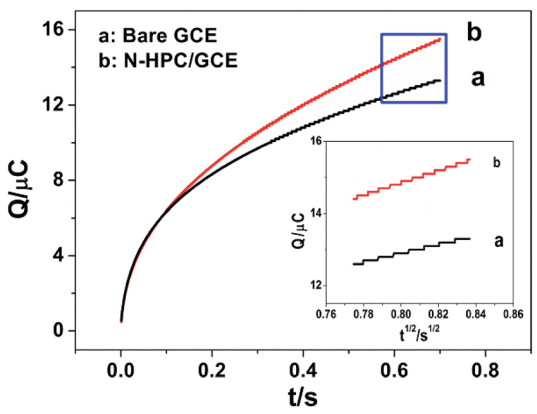

Fig. 3 The effective surface area curves of the bare GCE and the N-HPC/GCE as a function of time.

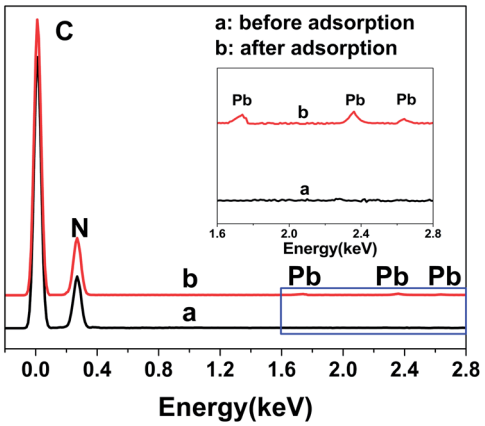

Fig. 5 The EDX spectrum of N-HPC before and after the adsorption of Pb^{2+}.

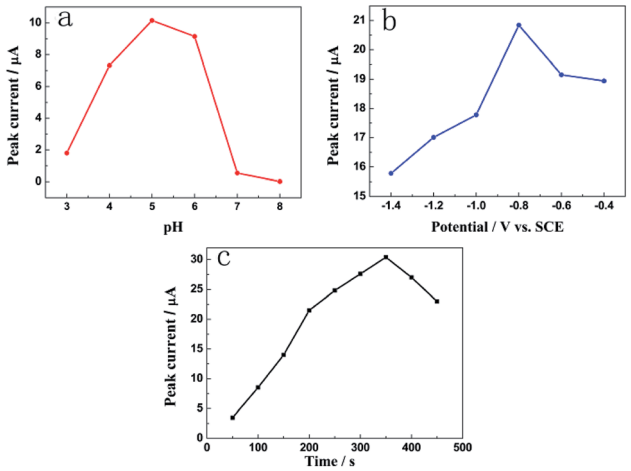

Fig. 6 The effects of (a) the pH of the acetate buffer solution; (b) deposition potential; and (c) deposition time on the current signal of Pb^{2+}.

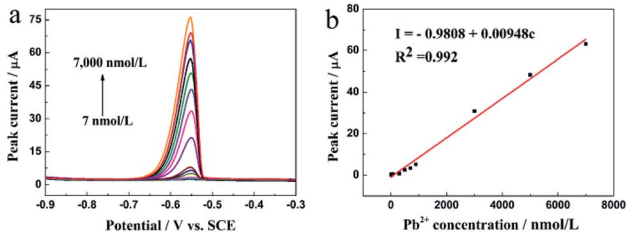

Fig. 7 (a) DPASV responses of the N-HPC/GCE for the detection of Pb^{2+} at different concentrations in the 0.1 M HAc–NaAc buffer solution at pH 5.0. DPASV conditions are identical to those shown in Fig. 4; and (b) the corresponding linear calibration plots of the current signal for Pb^{2+}.

However, after the deposition time exceeded 350 s, the peak current decreased gradually. Thus, the deposition time of 350 s was employed in the further studies taking into account the work efficiency and sensitivity of the sensor.

Analytical properties

The analytical properties of the N-HPC/GCE in the detection of Pb^{2+} were researched using DPASV under the optimal conditions. Fig. 7a demonstrates the peak current responses to Pb^{2+} at different concentrations in the 0.1 M HAc–NaAc buffer solution (pH 5.0). The anodic peak current was linearly correlated to the Pb^{2+} concentration in the range from 7.0 to 7000.0 nM ($R^2 = 0.992$), as shown in Fig. 7b. The corresponding equation is indicated as I (μA) = −0.9808 + 0.00948c (nM), and the detection limit is 1.44 nM (S/N = 3).

Table 1 shows a comparison of the performance of this modified electrode with those of other reported Pb^{2+} sensors. It can be seen that the N-HPC/GCE reported in this study has wider linear range than the previously reported materials. The detection limit of the proposed approach is lower than that of the RGO-NH-Ci/GCE and similar to that of TAPB-DMTP-COF/CPE. In addition, compared with TAPB-DMTP-COF/CPE, the proposed material has the advantages of easier preparation and lower cost. Moreover, N-HPC as the modification material of this sensor has a controllable and reproducible morphology, which can provide stability and sensitivity. Hence, the N-HPC/GCE is strongly expected to be used as a valid working electrode for Pb^{2+} detection.

Repeatability, reproducibility, stability and interference

To certify the repeatability, reproducibility and stability of the N-HPC/GCE, 5.0 μM Pb^{2+} was successively detected using the same electrode. After 10 continuous measurements, the relative standard deviation (RSD) of the N-HPC/GCE repeatability was 2.5%, as shown in Fig. S5A.† The reproducibility was examined using five different N-HPC/GCEs treated with the same method; the RSD of 3.2% for the N-HPC/GCE was determined based on Fig. S5B.† These results demonstrate that the designed sensor has good reliability. In addition, to assess the long-term stability of the N-HPC/GCE, 5.0 μM Pb^{2+} was measured after 15 days of storage in air. The current signal change in response to Pb^{2+} is less than 4%, indicating that the modified electrode has an excellent stability.

The anti-interference properties of different interfering substances in the HAc–NaAc buffer solution containing 5.0 μM Pb^{2+} were tested. From Fig. S5C,† it is found that the current signal change relative to the original signal for Pb^{2+} is within ±5.0%, which proves that 50-fold Co^{2+}, Ni^{2+}, Ca^{2+}, Mg^{2+}, Zn^{2+}, Mn^{2+}, and Al^{3+}, 20-fold Cd^{2+}, and 10-fold Hg^{2+} and Cu^{2+} have no

Table 1 Comparison of the analytical performance of the electrochemical methods for the determination of Pb^{2+}

Electrode	Method	Liner range (nM)	Determination limit (nM)	Reference
Poly(DTCPA)/GCE[a]	SWASV[b]	100–1000 000	—	28
TAPB-DMTP-COF/CPE[c]	DPASV	5–2000	1.9	8
Mn(TPA)-SWCNTs/GCE[d]	DPASV	100–14 000	38	29
L-cys-RGO/GCE[e]	DPASV	400–1200	1.04	30
RGO-NH-Ci/GCE	DPASV	5–1200, 1200–10 000	3.0	9
N-HPC/GCE	DPASV	7–7000	2.0	This work

[a] Poly(DTCPA)/GCE: poly(7,9-dithiophene-2yl-8*H*-cyclopenta[*a*] acenaphthalene-8-one)-modified GCE. [b] SWASV: square-wave adsorptive stripping voltammetry. [c] TAPB-DMTP-COF/CPE: 1,3,5-tris(4-aminophenyl)benzene-2,5-dimethoxyterephaldehyde-covalent organic framework-modified carbon paste electrode. [d] Mn(TPA)-SWCNTs/GCE: manganese-terephthalic acid MOF/single-walled carbon nanotube modified GCE. [e] L-cys-RGO/GCE: L-cysteine-reduced graphene oxide-modified GCE.

Table 2 Recovery of Pb^{2+} in waste water using the N-HPC/GCE electrode ($n = 3$)

Spiked (nM)	Founded (nM)	Recovery (%)
0	24.8	—
50	73.2	96.8
100	125.2	100.4
150	171.6	97.9

effect on the determination of Pb^{2+}. These results suggest that the N-HPC/GCE material has excellent selectivity that may be due to the high binding affinity of the NH_2^- groups towards Pb^{2+}.

Actual sample analysis

The sensor containing the N-HPC/GCE electrode was used to analyze Pb^{2+} in actual samples for testing its feasibility and validity. The waste water was filtered with a standard 0.45 μm filter, and the pH value was adjusted to 5.0 with the HAc–NaAc buffer solution before determination. Table 2 shows the Pb^{2+} recovery results in wastewater achieved using the N-HPC/GCE electrode by the standard addition method to assess the preciseness of the developed sensor. The Pb^{2+} recovery was determined to be between 96.8% and 100.4% by spiking the samples at three concentration levels (50 nM, 100 nM and 150 nM). The results demonstrate the accuracy of the prepared sensor for Pb^{2+} determination in actual samples.

Conclusions

In this study, a new electrochemical sensor was developed for the detection of Pb^{2+} based on nitrogen-doped hierarchical porous carbon (N-HPC), which was easily obtained by calcination of gelatin-based microcapsules with good repeatability and controllability. The N-HPC/GCE material presented a good linear response to the Pb^{2+} concentrations ranging from 7 nM to 7000 nM with the detection limit of 1.44 nM. The excellent sensitivity of the obtained method can be ascribed to the strong Pb^{2+} coordinating ability of the N atoms and large surface area of the N-HPC. In addition, the N-HPC-modified GCE exhibited good repeatability, reproducibility, stability, and selectivity and was successfully applied to the detection of Pb^{2+} in actual samples. These results suggested that the N-HPC/GCE electrochemical sensor might be a prospective candidate for the environmental monitoring of Pb^{2+}.

Conflicts of interest

There are no conflicts to declare.

Acknowledgements

This research was financially supported by the National Natural Science Foundation of China (Grant No. 21304039); the Science & Technology Program of Jiangxi Province (Grant No. 2013BAB213014); and the Department of Education Science & Technology Program of Jiangxi Province (Grant No. GJJ150405); Natural Science Foundation of Nanchang City (No. 2018CXTD014).

References

1 W. Kang, X. Pei, C. A. Rusinek, A. Bange, E. N. Haynes, W. R. Heineman and I. Papautsky, *Anal. Chem.*, 2017, **89**, 3345–3352.
2 M. A. Moreno, *JAMA Pediatr.*, 2018, **172**, 204.
3 W. H. Organization, *Guidelines for drinking-water quality*, WHO Press, Geneva, Switzerland, 4th edn, 2011.
4 V. Kazantzi, A. Kabir, K. G. Furton and A. Anthemidis, *Microchem. J.*, 2018, **137**, 285–291.
5 A. A. Krata, M. Wojciechowski, M. Kalabun and E. Bulsk, *Microchem. J.*, 2018, **142**, 36–42.
6 S. Tanikkul, J. Jakmune, S. Lapanantnoppakhun, M. Rayanakorn, P. Sooksamiti, R. E. Synovec, G. D. Christian and K. Grudpan, *Talanta*, 2004, **64**, 1241–1246.
7 Y. Ma, H. Liu, K. Qian, L. Yang and J. Liu, *J. Colloid Interface Sci.*, 2012, **386**, 451–455.
8 T. Zhang, C. Gao, W. Huang, Y. Chen, Y. Wang and J. Wang, *Talanta*, 2018, **188**, 578–583.
9 H. Xing, J. Xu, X. Zhu, X. Duan, L. Lu, Y. Zuo, Y. Zhang and W. Wang, *J. Electroanal. Chem.*, 2016, **782**, 250–255.
10 L. Yua, Q. Zhang, B. Yang, Q. Xua, Q. Xub and X. Hu, *Sens. Actuators, B*, 2018, **259**, 540–551.
11 S. Wu, Q. He, C. Tan, Y. Wang and H. Zhang, *Small*, 2013, **9**, 1160–1172.
12 H. Xing, J. Xu, X. Zhu, X. Duan, L. Lu, W. Wang, Y. Zhang and T. Yang, *J. Electroanal. Chem.*, 2016, **760**, 52–58.
13 A. T. E. Vilian, J. Y. Song, Y. S. Lee, S.-K. Hwang, H. J. Kim, Y.-S. Jun, Y. S. Huh and Y.-K. Han, *Biosens. Bioelectron.*, 2018, **117**, 597–604.
14 L. Wang, Q. Zhang, S. Chen, F. Xu, S. Chen, J. Jia, H. Tan, H. Hou and Y. Song, *Anal. Chem.*, 2014, **86**, 1414–1421.
15 N. Qiu, Y. Liu and R. Guo, *Electrochim. Acta*, 2016, **212**, 147–154.
16 W. Deng, X. Yuan, Y. Tan, M. Ma and Q. Xie, *Biosens. Bioelectron.*, 2016, **85**, 618–624.
17 M. J. Liu, F. Wei, X. M. Yang, S. A. Dong, Y. J. Li and X. J. He, *New Carbon Mater.*, 2018, **33**, 316–323.
18 L. L. Shen, J. P. Chen, Y. J. Bai, Z. C. Ma, J. Huang and W. Feng, *J. Food Sci.*, 2016, **81**, 2258–2262.
19 X. Yang, N. Gao, L. Hu, J. Li and Y. Sun, *J. Food Eng.*, 2014, **161**, 87–93.
20 R. Y. Dai, S. Y. You, L. M. Lu, Q. Liu, Z. X. Li, L. Wei, X. G. Huang and Z. Y. Yang, *Colloids Surf., A*, 2017, **530**, 13–19.
21 E. Duhoranimana, E. Karangwa, L. Lai, X. Xu, J. Yu, S. Xia, X. Zhang, B. Muhoza and I. Habinshuti, *Food Hydrocolloids*, 2017, **69**, 111–120.
22 R. Y. Dai, G. Wu, W. G. Li, Q. A. Zhou, X. H. Li and H. Z. Chen, *Colloids Surf., A*, 2010, **362**, 84–89.
23 Y. Qian, C. Wang and F. Gao, *Biosens. Bioelectron.*, 2015, **63**, 425–431.

24 Y. Qian, D. Tang, L. Du, Y. Zhang, L. Zhang and F. Gao, *Biosens. Bioelectron.*, 2015, **64**, 177–181.
25 F. C. Anson, *Anal. Chem.*, 1964, **36**, 932–934.
26 H. Xu, J. Gao and D. Jiang, *Nat. Chem.*, 2015, **7**, 905–912.
27 A. Afkhami, H. Bagheri, H. Khoshsafar, M. Saber-Tehran, M. Tabatabaee and A. Shirzadmehr, *Anal. Chim. Acta*, 2012, **746**, 98–106.
28 P. Kumar, S. Saravanan, K. Ranjith and P. C. Ramamurthy, *J. Appl. Electrochem.*, 2014, **44**, 133–139.
29 F. Cai, Q. Wang, X. Chen, W. Qiu, F. Zhan, F. Gao and Q. Wang, *Biosens. Bioelectron.*, 2017, **98**, 310–316.
30 S. Muralikrishna, K. Sureshkumar, T. S. Varley, D. H. Nagaraju and T. Ramakrishnappa, *Anal. Methods*, 2014, **6**, 8698–8705.